Journal of Environmental Chemical Engineering 5 (2017) 3690–3697

Contents lists available at ScienceDirect

Journal of Environmental Chemical Engineering

journal homepage: www.elsevier.com/locate/jece

Research Paper

Spinel manganites synthesized by combustion method: Structural characterization and catalytic activity in the oxidative degradation of organic pollutants

Alejandra S. Diez[a], Sofía Schlichter[a], Vojtech Tomanech[a], Elisa V. Pannunzio Miner[b], Mariana Alvarez[a,*], Mariana Dennehy[a]

[a] INQUISUR—Departamento de Química, Universidad Nacional del Sur, Avda. Alem 1253, B8000CPB, Bahía Blanca, Argentina
[b] INFIQC—CONICET, Dpto de Fisicoquímica, Fac. de Ciencias Químicas, Universidad Nacional de Córdoba, Ciudad Universitaria, X5000HUA, Córdoba, Argentina

ARTICLE INFO

Keywords:
Substituted manganites
Advanced oxidation processes
Persulfate
Peroxymonosulfate
Organic pollutants

ABSTRACT

Two spinel-type oxides, $CuMn_2O_4$ and $CoMn_2O_4$ were synthesized by a simple combustion method. The oxides were characterized by X-ray Diffraction, infrared spectroscopy, scanning electron microscopy and atomic absorption spectroscopy. The structures of the obtained oxides were refined by the Rietveld method. The obtained samples were tested in the catalytic degradation of phenol and methyl orange. Two different oxidants were employed: potassium persulfate and peroxymonosulfate. The catalytic activity was tested, as well as the degradation efficiencies. The best results were obtained with the copper substituted oxides, using oxone as oxidant. With this system, mineralization of total organic carbon (TOC) reached more than 94% within 120 min of reaction. For cobalt mixed oxides, the TOC mineralization reached as much as 68% in the same condition. The activation mechanisms for the different systems studied in this work are discussed and two different pathways are proposed depending on the oxidant and/or the substitution metal.

1. Introduction

The contamination of toxic organic pollutants in subsurface soil and groundwater has been subject of concern in recent years. Water treatment plays an important role in the awareness of the environment preservation. Different industrial activities (petrochemical, pharmaceutical, chemical, textile, among others) discharge hazardous organic products in water bodies, causing damage to the human health.

Among the different processes to treat organic pollutants, such as biodegradation [1,2] and classical adsorption [3,4], advanced oxidation processes (AOPs) have gained attention lately as an attractive alternative due to its high efficiency [5–7]. These processes are based on the generation of hydroxyl radicals (·OH), more effective oxidant species than the chemical reagents that are commonly employed for this purpose (ozone, H_2O_2, etc). Similar to OH radicals, sulfate radicals may react with organic compounds by electron transfer, hydrogen abstraction or addition mechanisms. These radicals can be produced through the activation of persulfate (PS) anion, $S_2O_8^{2-}$, or decomposition of peroxymonosulfate (PMS), HSO_5^-. The anions activation may be achieved by heat, chelated or not-chelated transition metals, hydrogen peroxide, and alkaline pH conditions. The efficiency, effectiveness and reaction products may vary among the different contaminants and activation methods.

Recently, manganese oxides [8,9] and metal transition mixed oxides [10–12] were tested as heterogeneous catalysts in the activation of PS and PMS for the degradation of pollutants as azo dyes and phenolic compounds. In the first case, it has been demonstrated that manganese oxides resulted in effective catalysts for generating sulfate radicals to degrade phenol, being their efficiency dependant on the oxidation state of manganese and on its redox potential. In the latter case, the spinel-type structures were used as successful catalysts for the degradation of Acid Orange II, through oxone activation at neutral pH. Co, Mn and Ni substitution improved the reactivity of the spinel oxide.

In order to gain more insight about the effect of metal substitution, in this study, two spinel-type oxides, $CuMn_2O_4$ and $CoMn_2O_4$ were synthesized by a simple combustion method and fully characterized. The structures of the obtained oxides were refined by the Rietveld method and the catalytic activity was evaluated in the degradation of two organic pollutants, methyl orange azo dye and phenol. The reactivity of the oxides in PS and PMS activation was also discussed.

* Corresponding author.
E-mail addresses: alvarezm@criba.edu.ar, alvarezm72@yahoo.com.ar (M. Alvarez).

http://dx.doi.org/10.1016/j.jece.2017.07.013
Received 7 April 2017; Received in revised form 3 July 2017; Accepted 4 July 2017
Available online 14 July 2017

2. Experimental

2.1. Manganite oxides preparation

Two manganite oxides ($CuMn_2O_4$ and $CoMn_2O_4$) were synthesized following the technique reported by Arul Dhas et al. and Lazarraga et al. [13,14]. For each synthesis, both $Co(NO_3)_2{\cdot}6H_2O$ or $Cu(NO_3)_2{\cdot}3H_2O$ and $Mn(NO_3)_2{\cdot}4H_2O$ (Merck, A. R. grade), and the fuel (refined saccharose) were weighted in 1:2:1 molar proportions, taken in a Pyrex dish and dissolved in a minimum amount of distilled water. A heating plate was used to concentrate the solution until ignition took place and produced a foamy, black powder of low density. The as-produced sample was divided in two batches in order to calcine them at different temperatures (400 °C and 900 °C). The yield of the reaction was ca. 100%.

The stoichiometric reactions are:

$$Co(NO_3)_{2(aq)} + 2Mn(NO_3)_{2(aq)} + C_{12}H_{22}O_{11(aq)} + yO_{2(g)} \rightarrow CoMn_2O_4 + 2N_{2(g)} + 2NO_{x(g)} + 12CO_{2(g)} + 11H_2O_{(g)}$$

$$Cu(NO_3)_{2(aq)} + 2Mn(NO_3)_{2(aq)} + C_{12}H_{22}O_{11(aq)} + yO_{2(g)} \rightarrow CuMn_2O_4 + 2N_{2(g)} + 2NO_{x(g)} + 12CO_{2(g)} + 11H_2O_{(g)}$$

where y = 5 + x.

2.2. Solids characterization

The metal content in the samples was determined by atomic absorption spectrometry (AAS) from total dissolution of 30 mg of the solids in 6 M HCl, at 80 °C, using a GBC Model B-932 atomic absorption spectrometer. Chemical analyses were made in duplicate.

The IR spectra of the substances as KBr pellets were recorded in the 4000 to 400 cm^{-1} range on a Nicolet Nexus FTIR spectrometer.

The morphology of the particle aggregates and their qualitative compositions were characterized using scanning electron microscopy (SEM) coupled with energy-dispersive spectroscopy (EDS) using a JEOL 8230 electron microprobe, housed at LAMARX-UNC.

The specific surface area of the catalysts was calculated by the BET method from the nitrogen adsorption isotherms obtained at 77 K using a Micromeritics ASAP 2020 Plus apparatus.

Powder X-ray diffraction (XRD) experiments were performed with a PANAnalytical X'Pert Pro diffractometer (operated at 40 kV and 40 mA) with $CuK\alpha_{1+2}$ radiation, between 10° and 130° (2θ), with a step size of 0.02° (2θ) and counting time of 10 s/step. Rietveld structural refinements were performed using the FULLPROF program [15]. Peak profiles were fitted using a pseudo-Voigt function.

2.3. Catalytic activity

The two synthesized catalysts calcined at 400 °C were evaluated in the degradation of two pollutants, methyl orange and phenol. The efficiency of two oxidant agents, potassium persulfate ($K_2S_2O_8$) and Oxone® ($KHSO_5{\cdot}½KHSO_4{\cdot}½K_2SO_4$), was also tested. The UV–vis spectra of the degradation experiments were registered using a Cecil 2021 spectrophotometer.

2.3.1. Methyl orange (MO) degradation

The degradation reactions were performed in a glass reactor, containing 150 mL of MO solution (10 mg L^{-1}) at 30 °C. The pH was adjusted to 3 with H_2SO_4. In a typical procedure, the reaction was initiated by adding oxidant and 50 mg of the catalyst into the prepared reaction solution. The mass ratio dye:oxidant:catalyst was 1:20:33. The reaction was held under mechanical stirring. At designated sampling intervals, aliquots of solution were removed from the reaction vessel. Immediately, the sampling was filtered with a syringe through a Nuclepore membrane (pore size 0.22 μm) and tested by the UV–visible spectrophotometer. The MO concentration at different reaction times was determined by measuring the absorption intensity at λ_{max} = 506 nm. Prior to the measurement, a calibration curve was obtained using MO solutions with known concentrations. The degradation efficiency of methyl orange was defined as follows:

$$\text{Degradationefficiency} = \left(1 - \frac{C_t}{C_0}\right) \times 100$$

where C_0 (mg L^{-1}) is the initial concentration of methyl orange, and C_t (mg L^{-1}) is the concentration of methyl orange at reaction time, t (min).

2.3.2. Phenol degradation

100 mg of catalyst were equilibrated in a glass reactor, containing 150 mL of phenol solution (60 mg L^{-1}) at 30 °C. The initial pH of the solution was 5.4. After that, adequate quantities of oxidant were mixed with the oxide suspension. The initial mass ratio phenol:oxidant:catalyst was 1:55.5:11.2. Samples were taken out at regular intervals and filtered in the same way as described above. The supernatant was then used for the analysis through an UV–vis full wavelength scanning.

The degree of mineralization of both pollutants were evaluated by measurements of total organic carbon (TOC), using a TOC-LCPH/CPN analyzer (Shimadzu). The pH was monitored with an Orion 250Aplus pHmeter equipped with a pH electrode.

The leaching of Co, Cu and Mn ions in the solutions were also determined with a GBC Avanta B-932 Atomic Absorption Spectrometer.

For recycled catalyst tests, the oxides were collected by filtration after reaction, washed with water and dried overnight for reuse test, keeping constant the oxidant:pollutant:catalyst mass ratio.

Quenching experiments were performed in the same experimental conditions, being the only difference the addition of ethanol (mass ratio pollutant:alcohol 1:250).

3. Results and discussion

3.1. X-Ray diffraction and Rietveld refinement

XRD patterns of the two obtained solids calcined at 900 °C are presented in Fig. 1, together with the refined patterns and their differences.

For sample $CuMn_2O_4$, the product obtained by calcined at 400 °C corresponds to a cubic spinel phase (88 wt.%) with a lattice parameter a of 0.82853 nm (Table 1), in good agreement with values reported in the literature [16]. Additional peaks indicate the presence of hausmannite ($MnMn_2O_4$, tetragonal). The content of this second phase was 12 wt%, and may be interpreted as a segregation of a Mn-rich spinel. When the calcination temperature was raised to 900 °C, the product crystallinity seemed to be higher (as indicated by narrower and higher peaks) but the segregation effect was more pronounced, with 20 wt% $MnMn_2O_4$. The tetragonal phase is attributed to the presence of Mn^{3+} ions (produced by oxidation of reagent Mn^{2+}) in octahedral sites. The Mn^{3+} ions distort the cubic spinel structure by deforming the octahedra via Jahn-Teller interactions. For $CoMn_2O_4$, experimental runs yielded a single phase, regardless of calcination temperature. The lattice parameters (Table 3) are also in good agreement with the literature [17,18].

Cell parameters, agreement factors, refined atomic coordinates and calculated main interatomic distances and angles are summarized in Tables 1–6.

The vibrational spectra of $CoMn_2O_4$ and $CuMn_2O_4$ spinels can be seen in Fig. S1 (Supplementary material). In general, spinel type compounds present two main metal-oxygen bands. The spectrum of $CoMn_2O_4$ is typical for a Co-Mn spinel. The bands at around 608 cm^{-1} can be assigned to the vibrational bending modes of the atoms in the tetrahedral oxygen environment (mainly cobalt), while those around 502 cm^{-1} can be related to the vibration of the atoms in the octahedral

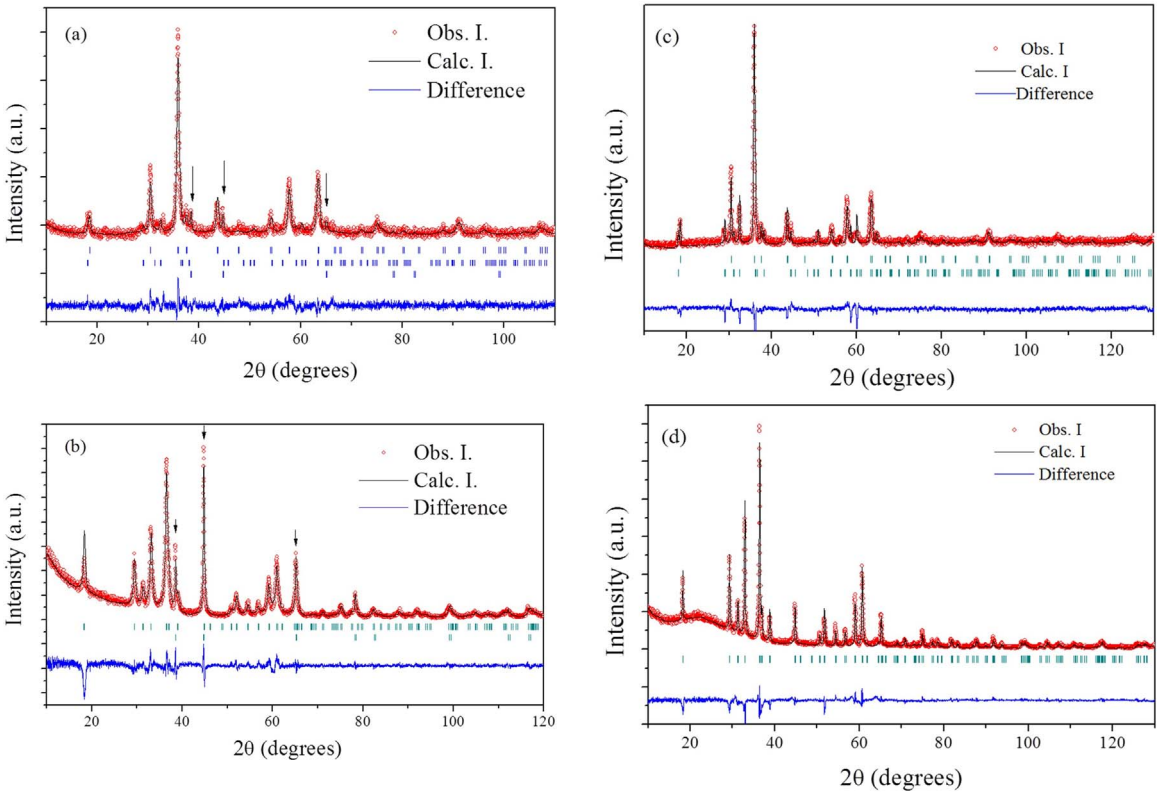

Fig. 1. – XRD patterns and Rietveld fits of experimental products (a) $CuMn_2O_4$ and (b) $CoMn_2O_4$, calcined at 400 °C (c) $CuMn_2O_4$ and (d) $CoMn_2O_4$, calcined at 900 °C. Measured (red dots) and calculated (black line) intensities, and their differences (blue line, bottom), Short vertical lines (light blue) indicate the Bragg positions for $CuMn_2O_4$, $MnMn_2O_4$ and $CoMn_2O_4$. (For interpretation of the references to colour in this figure legend, the reader is referred to the web version of this article.).

Table 1
Miscellaneous crystallographic data and structure refinement parameters for $CuMn_2O_4$.

Calcination temperature (°C)	400		900	
Phases	$Cu_{1.5}Mn_{1.5}O_4$	Mn_3O_4	$Cu_{1.5}Mn_{1.5}O_4$	Mn_3O_4
Percentage (wt.%)	88	12	80	20
Crystal system	Cubic	Tetragonal	Cubic	Tetragonal
Space group (number)	*Fd*–3 *m* (#227)	$I4_1/amd$ (#141)	*Fd-3m* (#227)	$I4_1/amd$ (#141)
a (nm)	0.82853(8)	0.57525(9)	0.82854(7)	0.57524(2)
c (nm)		0.94142(3)		0.94143(2)
V (nm^3)	0.56875(1)	0.31153(9)	0.56877(1)	0.31152(7)
Crystallite size (nm)	18.9	–	26.2	–
Goodness-of-fit parameters	Calcination temperature 400 °C		900 °C	
R_P	7.0		6.1	
R_{WP}	10.1		7.6	
R_{exp}	5.9		4.7	
χ^2	2.96		2.65	

oxygen environment (mainly manganese). These values are similar to those reported by Hosseini et al. [19]. For the copper spinel, $CuMn_2O_4$, the vibration frequencies of M-O also appear below 1000 cm^{-1}. Three vibrational frequencies at 609, 522 (shoulder) and 501 cm^{-1} confirm the formation of M-O (Cu-O and Mn-O) bonds. The band exhibited at

Table 3
Distances and angles for $Cu_{1.5}Mn_{1.5}O_4$.

	Distances (nm)	Angles (degrees)
(Mn1)-O (×6)	0.20071(2)	
O-(Mn1)-O		109.07(7)
(Mn2,Cu1)-O	0.19788(2)	
O-(Mn2,Cu1)-O		180.0(1)

Table 4
Miscellaneous crystallographic data and structure refinement parameters for $CoMn_2O_4$.

Calcination temperature (°C)	400	900
Phase	$CoMn_2O_4$	$CoMn_2O_4$
Percentage (wt.%)	100	100
Crystal system	Tetragonal	Tetragonal
Space group (number)	$I4_1/amd$ (#141)	$I4_1/amd$ (#141)
a (nm)	0.57233(7)	0.57517(5)
c (nm)	0.9261(1)	0.9277(2)
V (nm^3)	0.30335(2)	0.30371(4)
Crystallite size (nm^3)	15.1	58.4
Goodness-of-fit parameters	Calcination temperature 400 °C	900 °C
R_{WP}	15.8	13.9
R_{exp}	9.7	7.3
χ^2	3.22	3.01

Table 2
Fractional atomic positional coordinates, isotropic atomic displacement parameters and site occupation factors (sof) for $Cu_{1.5}Mn_{1.5}O_4$.

Site	Atom	Wyckoff position	*x*	*y*	*z*	sof	B_{iso} (400 °C)	B_{iso} (900 °C)
O1	O^{2-}	32e	0.2552(2)	0.2552(2)	0.2552(2)	1	1.14(3)	1.65(2)
Mn1	Mn^{3+}	8a	1/8	1/8	1/8	1	0.81(2)	0.78(2)
Mn2	Mn^{4+}	16d	1/2	1/2	1/2	0.33	0.93(2)	0.73(2)
Cu1	Cu^{2+}	16d	1/2	1/2	1/2	0.66	0.93(2)	0.73(2)

Table 5
Fractional atomic positional coordinates, isotropic atomic displacement parameters and site occupation factors (sof) for $CoMn_2O_4$.

Site	Atom	Wyckoff position	x	y	z	sof	B_{iso} (400 °C)	B_{iso} (900 °C)
O1	O^{2-}	32e	0	0.52	0.239	1	1.44(4)	1.30(4)
Mn1	Mn^{2+}	8a	0	1/4	0.375	0.8	0.65(3)	0.59(2)
Co1	Co^{2+}	8a	0	1/4	0.375	0.2	0.65(3)	0.59(2)
Mn2	Mn^{3+}	16d	0	0	0	0.8	0.78(7)	0.66(2)
Co2	Co^{3+}	16d	0	0	0	0.2	0.78(7)	0.66(2)

Table 6
Distances and angles for $CoMn_2O_4$.

	Distances (nm)	Angles (degrees)
(Mn1,Co1)-O	0.19766(2)	
O-(Mn1,Co1)-O		107.03(9)
(Mn2,Co2)-O	0.19788(2)	
O-(Mn2,Cu1)-O		180.0(1)

609 cm^{-1}can be assigned to the Cu^{2+} ions mainly in the octahedral sites. The two bands at 522/501 cm^{-1} could be attributed to both octahedral and tetrahedral Mn ions [20].

3.2. Morphology

SEM micrographs of the spinels obtained by combustion synthesis at 400 °C and at 900 °C are shown in Fig. 2. All samples revealed porous structures and rough surfaces. These features could be a consequence of the high contents of gas that evolved during the combustion process.

Table 7
BET surface area (m^2/g).

Sample	400 °C	900 °C
$CuMn_2O_4$	15.3 ± 0.1	1.68 ± 0.04
$CoMn_2O_4$	12.33 ± 0.07	3.0 ± 0.1

The BET surface area of the samples is shown in Table 7. As can be seen from the values, the increase of the calcination temperature caused a decrease in the specific surface area. Even though the surface area values are rather low as compared with traditional catalysts, the high yield obtained indicate that they are suitable for the studied reactions from a practical point of view.

3.3. Catalytic activity

3.3.1. MO degradation

Initially, in order to evaluate the individual effect of catalysts and oxidants on MO removal preliminary experiments were carried out, including adsorption test of dye molecules on the catalysts surface and non-catalytic, chemical oxidation with oxidants alone. A control test using only PS and PMS at pH 3 showed slight changes in the MO concentration. Less than 20% color removal was reached after 120 min when PS was tested and a degree of decolorization close to 100% when PMS was evaluated. However, in the latter case, the UV band

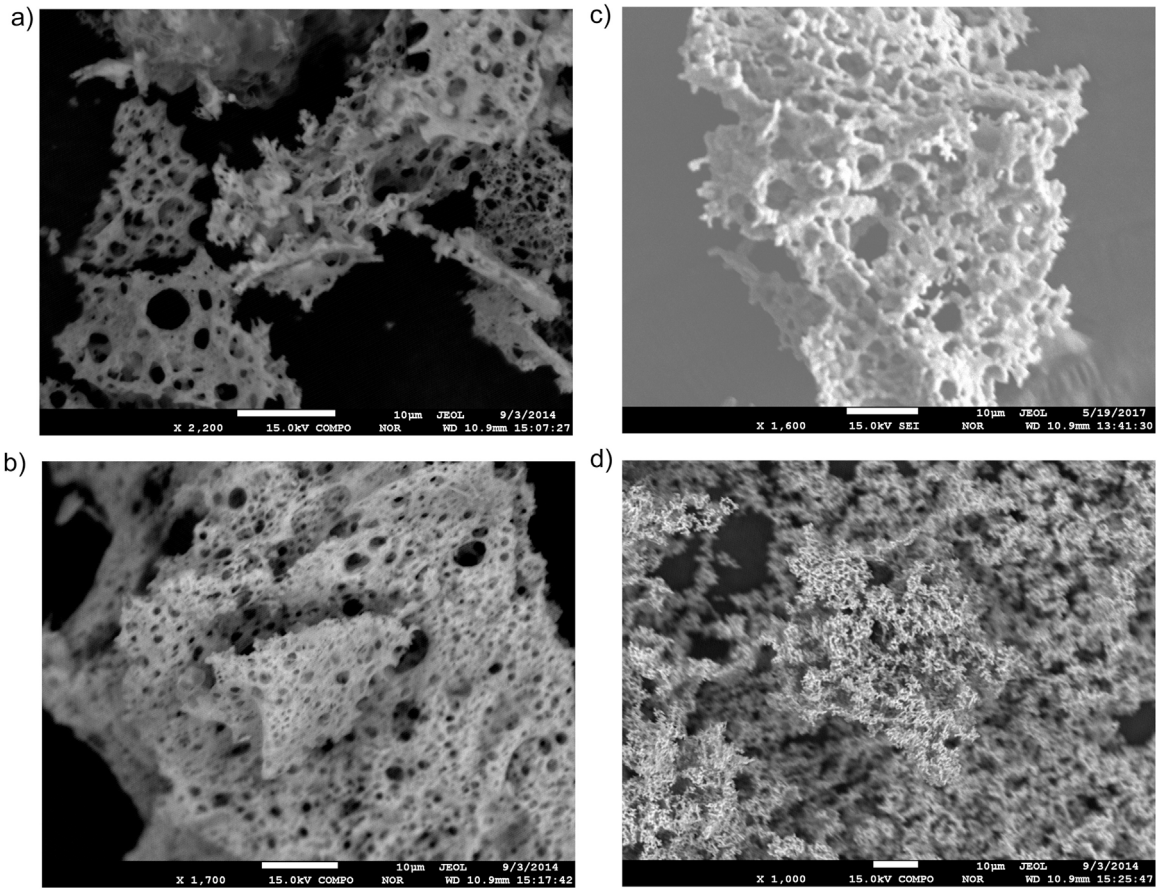

Fig. 2. – SEM micrographs of (a) $CuMn_2O_4$ and (b) $CoMn_2O_4$, calcined at 400 °C (c) $CuMn_2O_4$ and (d) $CoMn_2O_4$, calcined at 900 °C.

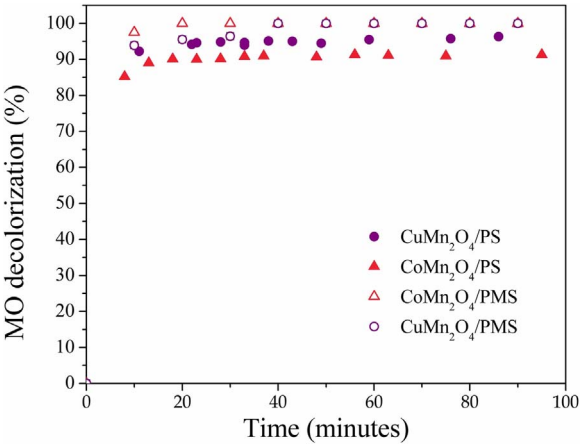

Fig. 3. – MO catalytic decolorization profiles.

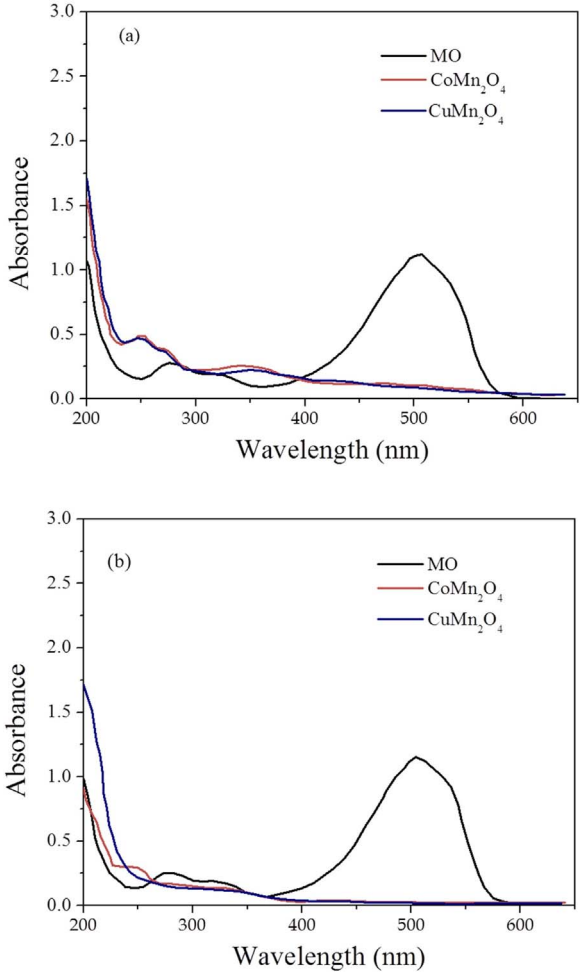

Fig. 4. – UV profiles of MO degradation with both catalysts after 120 min reaction. (a) PS, (b) PMS.

corresponding to the aromatic ring was still present with high intensity after 120 min reaction, indicating that even if the azo bond was broken, secondary products of the reaction were still present and the complete mineralization did not occur.

In the presence of bulk catalysts and without oxidant addition, a significant decrease of colorization was observed. After 250 min of reaction, aromatic compounds were still in solution (checked by UV spectroscopy, see Fig. S2 (Supplementary material)). This could be due to the partial dye elimination by an adsorption process, although the degree of pollutant removal seems to be less efficient than through an oxidation route.

Table 8
Percentage of Mineralization of MO after 120 min of reaction, based on TOC results.

Persulfate		Peroxymonosulfate	
$CoMn_2O_4$	$CuMn_2O_4$	$CoMn_2O_4$	$CuMn_2O_4$
37.0%	28.0%	37.1%	47.1%

Fig. 3 displays the MO degradation profiles in different systems, comprising combination of oxidants and bulk catalysts: $CuMn_2O_4$ and $CoMn_2O_4$. Results depicted in Fig. 3 clearly show that simultaneous presence of catalysts and oxidants led to significant decolorization of the MO.

Color removal of MO as high as 92% could be achieved within a short period of 10 min (for $CuMn_2O_4$ with PS) and > 97% for Co and Cu-based catalysts with PMS, despite the very low catalysts concentrations (0.67 g/L) used in reaction. Fig. 4 shows the UV profiles of MO initial solution and the evolution of the oxidation after 2 h reaction with both Cu and Co-based catalysts, and both oxidants.

As shown in Fig. 4(a and b), the initial UV–vis spectrum of MO solution shows characteristic bands at 506, 321 and 278 nm. The first band is attributed to the N=N group of the azo bond, while the latter two correspond to the modification of the π system delocalization. The temporal evolution of the UV–vis spectrum of MO in the catalysts/oxidant system shows that the band located at 506 nm disappeared after 120 min of reaction, without the appearance of new absorption bands in the visible region. This reflects that the decolorization of the MO solution was practically complete in all cases. However, the spectra in the range of 200–300 nm show that MO was not completely mineralized, even though the absorption intensity was reduced in that range. This fact was further confirmed by TOC results (Table 8).

The latter results proved that the faster and complete removal of MO from the solution under heterogeneous oxidation process is due to its catalytic transformation rather than to the adsorption of the dye molecules on the catalysts surface. Under the same operating conditions, spinel oxides exhibited a major catalytic activity when PMS was used as oxidant agent, being the more efficient catalyst the $CuMn_2O_4$ spinel.

Scarce results were found in the literature regarding the methyl orange degradation with Co-Mn and Cu-Mn spinels, as catalysts, in AOP processes. Yao et al. [21] studied the removal of different azo dyes with $MnFe_2O_4$ catalyst obtained by co-precipitation method with PMS as oxidant. They found that the removal of Orange II had an efficiency of around 90%, with a 20 ppm solution, employing a different catalyst:oxidant ratio.

3.3.2. Phenol degradation

Adsorption tests showed that the oxides presented no adsorption of phenol, after 240 min of reaction. In the catalytic oxidation tests, addition of oxidants without the presence of a catalyst did not induce phenol oxidation reaction. Phenol degradation would only occur when oxide catalyst and oxidants, PS (Fig. 5) or PMS (Fig. 6) were simultaneously present in the solution. Before treatment, the UV–vis spectrum of phenol exhibited a main absorption band in the UV region, < 300 nm. As the reaction advanced, in some cases a band in the visible region appeared, with variable intensity, and then disappeared after 300 min of reaction. Thus, the absorption region confirms the development of color, in agreement with the observations reported by Mijangos et al.

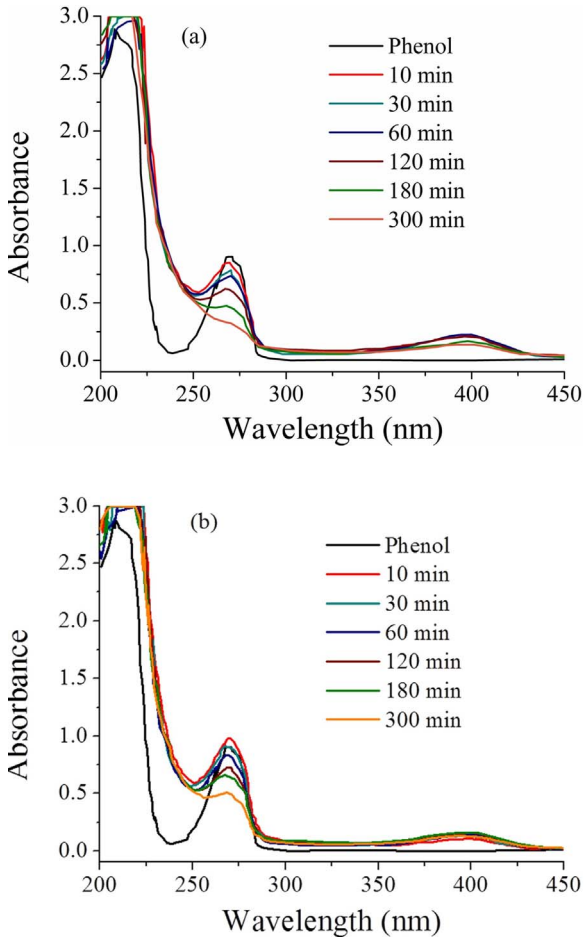

Fig. 5. – UV–vis spectra of phenol degradation of (a) $CoMn_2O_4$ and (b) $CuMn_2O_4$, with PS as oxidant.

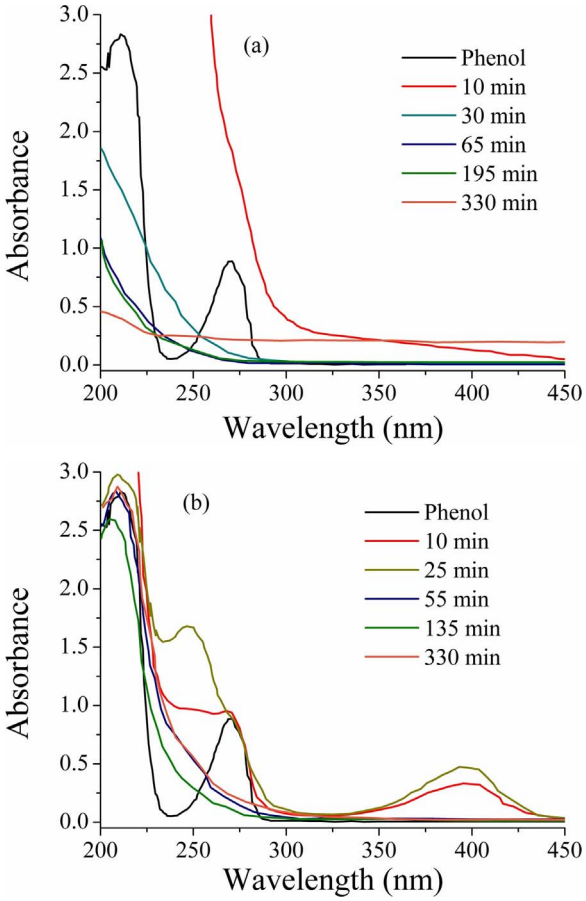

Fig. 6. – UV–vis spectra of phenol degradation of (a) $CoMn_2O_4$ and (b) $CuMn_2O_4$, with PMS as oxidant.

[22] and Lin et al. [23]. They postulated that the color development could be attributed to a mix of intermediate compounds including *p*-benzoquinone (yellow), o-benzoquinone (red) and hydroquinone (colorless).

The phenol degradation was also confirmed by the reduction of TOC of the solution (Table 9). The TOC degradation clearly shows that the mineralization of phenol is high, and almost completed when the copper spinel was used as catalyst in the presence of PMS.

In a comparison of all catalysts performances, $CuMn_2O_4$ seems to be more effective in activating PMS to generate sulfate radicals. This result is in some way unexpected, because it has been postulated that the best combination for $SO_4^{\cdot -}$ generation is Co/PMS [24]. In this work, the synergistic effect of Mn with Cu resulted in better results for phenolic pollutant degradation.

Previous studies in the literature [25,26], also reported high removal percentage of phenol in aqueous solution (> 90%) using mixed Co-Fe spinel systems. However, the authors employed higher oxidant amounts (PMS) and lower phenol concentration than those used in our study.

3.4. Catalyst stability

The stability of $CuMn_2O_4$ and $CoMn_2O_4$ catalysts were examined through reuse experiments. The results, expressed as% TOC removal, are presented in Fig. 7. During the recycling experiments with PMS, the catalytic activity of the $CuMn_2O_4$ oxide towards phenol degradation slightly decreased in the second run of use, with > 86% of phenol removal after 120 min reaction. In a third run, the activity slightly increased again, reaching a phenol removal > 94%. These results evidently point out that if there are any reaction intermediates on the catalyst surface they can be detached by water washing process at room temperature.

Regarding the Co-Mn mixed spinel, the catalytic activity was practically constant after the second run of use (68% at 120 min of reaction). An increase in the phenol elimination was measured in the third run (from 68% to 83%). It is known that manganese has the capacity to form species of different oxidation states, and the reactivity of the catalysts is associated with the ability of convert one into other on the solid surface [8]. These results could be suggesting that an electronic

Table 9
Percentage of mineralization of phenol, based on TOC results.

Catalyst		Persulfate	Peroxymonosulfate
$CoMn_2O_4$	120 min	48.4%	68.1%
	300 min	69.1%	73.1%
$CuMn_2O_4$	120 min	34.9%	94.2%
	300 min	58.0%	95.6%

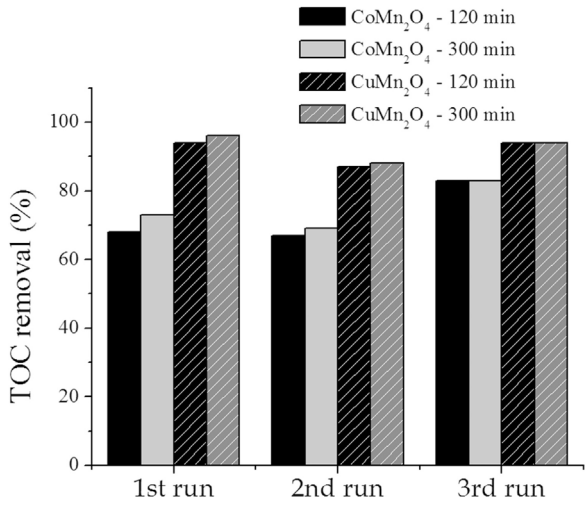

Fig. 7. – The reusability of the spinel catalysts in phenol oxidation.

transfer occurs through the oxide surface, regenerating the active sites.

3.5. Reaction mechanisms involved in the oxidant activation

The performance of various Co and Cu mixed metal catalysts as PS and PMS activators have been subject of many investigations [3,5,27–29]. Compared to the bare manganese spinels [2,30], Co and Cu mixed metal oxides exhibited better catalytic activity and stability for the removal of organic pollutants in wastewater.

Based on a similar system proposed in [12], in which superficial Co and Mn ions act as Lewis sites and dissociate adsorbed water molecules to generate hydroxylated metal sites ($\equiv Me^{II} - {}^{-}OH$), the MO degradation by $CoMn_2O_4$/PMS system can be summarized as follows:

$$\equiv Co^{II} + HSO_5^- \rightarrow \equiv Co^{III} + SO_4^{2-} + HO$$

$$\equiv Mn^{II} + HSO_5^- \rightarrow \equiv Mn^{III} + SO_4^{2-} + HO$$

$$\equiv Co^{II} - {}^{-}OH + HSO_5^- \rightarrow \equiv Co^{III} - {}^{-}OH + SO_4^{-\cdot} + OH^-$$

$$\equiv Co^{III} - {}^{-}OH + HSO_5^- \rightarrow \equiv Co^{II} - {}^{-}OH + SO_5^{-\cdot} + H^+$$

$$\equiv Mn^{II} - {}^{-}OH + HSO_5^- \rightarrow \equiv Mn^{III} - {}^{-}OH + SO_4^{-\cdot}$$

$$\equiv Mn^{III} - {}^{-}OH + HSO_5^- \rightarrow \equiv Mn^{II} - {}^{-}OH + SO_5^{-\cdot} + H^+$$

$$\equiv Mn^{II} + Co^{III} \rightarrow \equiv Mn^{III} + Co^{II} \quad \Delta E^0 = +0.30\ V$$

$$SO_4^{-\cdot} + H_2O \rightarrow HO + HSO_4^-$$

$SO_4^{-\cdot}$ (and/or HO) + Methyl orange → degradation intermediates → $CO_2 + H_2O$

The following equations summarize the schematic steps of the mechanism of PMS activation by $CuMn_2O_4$:

$$\equiv Cu^{II} + HSO_5^- \rightarrow \equiv Cu^{I} + SO_5^- + H^+$$

$$\equiv Mn^{III} + Cu^{I} \rightarrow \equiv Mn^{II} + Cu^{II} \quad \Delta E^0 = +1.34\ V$$

It is clear that the reduction of Mn^{III} by Cu^{I} is thermodynamically favorable, and this fact may result in more active sites on the catalyst and contribute to the catalytic activity of the mixed oxide.

The reaction mechanism of phenol degradation depended on the used catalyst and on the oxidant. During the first steps of the degradation, phenol reacted to produce aromatic compounds (hydroquinone, benzoquinone) giving rise to a color change, as it was demostrated by the appearance of a band in the visible region in Fig. 5 for both Cu/PS and Co/PS systems, and Fig. 6(b) for Cu/PMS system. These intermediates were subsequently mineralized to CO_2 and H_2O. At the end of the reaction, the residual solution was colorless. In the case of Co/PMS (Fig. 6(a)), the activation of the oxidant by Co^{2+} seems to be more efficient, in agreement with data reported in the literature [21,31]. The absence of the visible band in the spectrum indicates that the mechanism could be occurring by a fast and almost undetectable degradation of the aromatic intermediates up to the mineralization.

The reaction mechanism of oxidants activation by all the metals involved (Cu^{2+}, Mn^{3+} and Co^{2+}) could be described as follows:

With PMS:

$$Me^{n+} + HSO_5^- \rightarrow Me^{(n+1)+} + SO_4^{\cdot -} + OH^-$$

$$Me^{(n+1)+} + HSO_5^- \rightarrow Me^{n+} + SO_5^{\cdot -} + H^+$$

With PS:

$$Me^{n+} + S_2O_8^{2-} \rightarrow Me^{(n+1)+} + SO_4^{\cdot -} + SO_4^{2-}$$

$$Me^{n+} + SO_4^{\bullet -} \rightarrow Me^{(n+1)+} + SO_4^{2-}$$

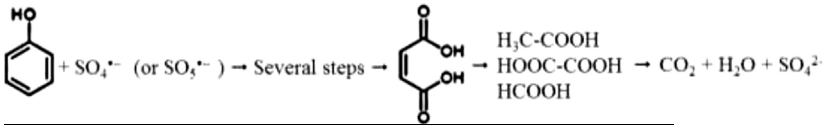

Oxalic acid is one of the intermediates of phenol that is refractory to oxidation [32], and may be the responsible of the residual TOC and the drop of pH after reaction (from almost 6 for the initial phenol solution to around 4 for the residual liquid).

Quenching experiments were performed with the addition of ethanol in order to verify the primary radicals species involved in the pollutants degradation. Literature information [31] suggests that alcohols with alpha-H, such as CH_3CH_2OH readily react with hydroxyl and sulfate radicals. Peroxymonosulfate radicals, however, are relatively inert towards alcohols. Regarding the degradation of MO, the UV profiles did not change after the addition of ethanol, for both catalysts and oxidants. This result would indicate that the oxidant activation at the reaction pH (3) is mainly directed by peroxymonosulfate radicals. For phenol removal, on the other hand, appreciable inhibition in the transformation of the pollutant was observed in all cases. This result is in agreement with Anipsitakis and Dionysiou [31] suggesting that sulfate/hydroxyl radicals are the major species responsible for the phenol transformation.

5. Conclusions

Two powders of metal spinels, $CoMn_2O_4$ and $CuMn_2O_4$ were prepared and characterized. Their performance in the activation of PS and PMS to degrade organic contaminants were tested. A simple method of preparation by combustion was carried out. The results showed that a mixed phase for Cu-Mn system was obtained when the combustion temperature was raised. Rietveld refinements were performed, and samples calcined at 400 °C were tested in the oxidative degradation of

methyl orange and phenol solutions. In both cases, the best performance was reached by $CuMn_2O_4$/PMS system. For MO degradation TOC values up to 47% were reached after 120 min of reaction. The efficiency to remove phenol reached levels of mineralization > 95%. The catalysts stabilities were evaluated after three reuse cycles and the efficiency was kept in values above 90% up to the third run.

Conflict of interest

The authors have declared no conflict of interest.

Acknowledgements

The authors gratefully acknowledge Lic. Rodolfo Dionisi and Lic. Claudio Vanina for their generous cooperation in the TOC measurements. This project was supported by SGCyT-UNS (Project M24/Q075).

Appendix A. Supplementary data

Supplementary data associated with this article can be found, in the online version, at http://dx.doi.org/10.1016/j.jece.2017.07.013.

References

[1] J. Chakraborty, S. Das, Molecular perspectives and recent advances in microbial remediation of persistent organic pollutants, Environ. Sci. Pollut. R. 23 (2016) 16883–16903.
[2] D. Ghosal, S. Ghosh, T.K. Dutta, Y. Ahn, Current state of knowledge in microbial degradation of polycyclic aromatic hydrocarbons (PAHs): a review, Front. Microbiol. 7 (2016) 1369, http://dx.doi.org/10.3389/fmicb.2016.01369.
[3] A. Carmalin Sophia, E.C. Lima, N. Allaudeen, S. Rajan, Application of graphene based materials for adsorption of pharmaceutical traces from water and wastewater—a review, Desalination Water Treat. 57 (2016) 27573–27586.
[4] A. Ayati, M.N. Shahrak, B. Tanhaei, M. Sillanpää, Emerging adsorptive removal of azo dye by metal–organic frameworks, Chemosphere 160 (2016) 30–44.
[5] F. Ghanbari, M. Moradi, Application of peroxymonosulfate and its activation methods for degradation of environmental organic pollutants: Review, Chem. Eng. J. 310 (2017) 41–62.
[6] B. Bethi, S.H. Sonawane, B.A. Bhanvase, S.P. Gumfekar, Nanomaterials-based advanced oxidation processes for wastewater treatment: a review, Chem. Eng. Process.: Process Intensif. 109 (2016) 178–189.
[7] S. Schlichter, A.S. Diez, M.C. Zenobi, M. Dennehy, M. Alvarez, Multi-Metal-Substituted-Goethite as an effective catalyst for Azo Dye wastewater oxidation, Clean Soil Air Water 44 (2016) 1652–1660.
[8] E. Saputra, S. Muhammad, H. Sun, H.-M. Ang, M.O. Tadé, S. Wang, Manganese oxides at different oxidation states for heterogeneous activation of peroxymonopersulfate for phenol degradation in aqueous solutions, Appl. Catal. B 142–143 (2013) 729–735.
[9] Y. Li, L.-D. Liu, L. Liu, Y. Liu, H.-W. Zhang, X. Han, Efficient oxidation of phenol by persulfate using manganite as catalyst, J. Mol. Catal. A: Chem. 411 (2016) 264–271.
[10] G. Wei, X. Liang, Z. He, Y. Liao, Z. Xie, P. Liu, S. Ji, H. He, D. Li, J. Zhang, Heterogeneous activation of oxone by substituted magnetites $Fe_{3-x}M_xO_4$ (Cr, Mn, Co, Ni) for degradation of Acid Orange II at neutral pH, J. Mol. Catal. A: Chem. 398 (2015) 86–94.
[11] X. Li, Z. Wang, B. Zhang, A. Rykov, M.A. Ahmed, J. Wang, Fe_x $Co_{3-x}O_4$ nanocages derived from nanoscale metal-organic frameworks for removal of bisphenol A by activation of peroxymonosulfate, Appl. Catal. B 181 (2016) 788–799.
[12] Y. Yao, Y. Cai, G. Wu, F. Wei, X. Li, H. Chen, S. Wang, Sulfate radicals induced from peroxymonosulfate by cobalt manganese oxides (Co_xMn_3-xO_4) for Fenton-like reaction in water, J. Hazard. Mater. 296 (2015) 128–137.
[13] M.G. Lazarraga, L. Pascual, H. Gadjov, D. Kovacheva, b K. Petrov, J.M. Amarilla, R.M. Rojas, M.A. Martin-Luengo, J.M. Rojo, Nanosize $LiNi_yMn_2$ − $_yO_4$ ($0 \le y \le 0.5$) spinels synthesized by a sucrose-aided combustion method. Characterization and electrochemical performance, J. Mater. Chem. 14 (2004) 1640–1647.
[14] N. Arul Dhas, K.C. Patil, Combustion synthesis and properties of fine particle spinel, J. Solid State Chem. 102 (1993) 440–445.
[15] J. Rodríguez-Carbajal, Recent advances in magnetic structure determination by neutron powder diffraction, Phys. B 192 (1993) 55–69.
[16] A. Waskowska, J. Staun Olsen, L. Gerward, S. Steenstrup, E. Talik, $CuMn_2O_4$: properties and the high-pressure induced Jahn-Teller phase transition, J. Phys.: Condens. Matter 13 (2001) 2549–2562.
[17] N. Yamamoto, S. Kawano, N. Norio, S.-N. Higashi, Preparation by a wet method and ionic distribution of transition metal-substituted hausmannite spinel, Funtai oyobi Funmatsu Yakin 30 (1983) 48–54.
[18] M. Prabu, P. Ramakrishnan, S. Shanmugam, $CoMn_2O_4$ nanoparticles anchored on nitrogen-doped graphene nanosheets as bifunctional electrocatalyst for rechargeable zinc–air battery, Electrochem. Commun. 41 (2014) 59–63.
[19] S. Ali Hosseini, D. Salari, A. Niaei, F. Deganello, G. Pantaleo, P. Hojati, Chemical-physical properties of spinel $CoMn_2O_4$ Nano-powders and catalytic activity in the 2-propanol and Toluene combustion: effect of the preparation method, J. Environ. Sci. Health Part A 46 (2011) 291–297.
[20] M. Kharroubi, B. Gillot, R. Legros, R. Metz, A.C. Vajpei, A. Rousset, An IR spectroscopic investigation of copper manganite $CuxMn_{3-x}O_4$ ($O < x < ;1$) spinels and their oxidation products, J. Less Common. Metals 175 (1991) 279–287.
[21] Y. Yao, Y. Cai, F. Lu, F. Wei, X. Wang, S. Wang, J. Hazard. Mater. 270 (2014) 61–70.
[22] F. Mijangos, F. Varona, N. Villota, Changes in solution color during phenol oxidation by Fenton reagent, Environ. Sci. Technol. 40 (2006) 5538–5543.
[23] Y.-T. Lin, Ch. Liang, J.-H. Chen, Feasibility study of ultraviolet activated persulfate oxidation of phenol, Chemosphere 82 (2011) 1168–1172.
[24] G.P. Anipsitakis, D.D. Dionysiou, M.A. Gonzalez, Cobalt-mediated activation of peroxymonosulfate and sulfate radical attack on phenolic compounds. Implications of chloride ions, Environ. Sci. Technol. 40 (2006) 1000–1007.
[25] Y. Yao, Z. Yang, D. Zhang, W. Peng, H. Sun, S. Wang, Ind. Eng. Chem. Res. 51 (2012) 6044–6051.
[26] F.X. Qin, S.Y. Jia, Y. Liu, X. Han, H.T. Ren, W.W. Zhang, J.W. Hou, S.H. Wu, Mater. Lett. (2013).
[27] B. Viswanathan, V. Subramanian, J.S. Lee, Materials and Processes for Solar Fuel Production, Springer, New York, 2014.
[28] Y. Feng, D. Wu, Y. Deng, T. Zhang, K. Shih, Sulfate radical-mediated degradation of sulfadiazine by $CuFeO_2$ rhombohedral crystal-catalyzed peroxymonosulfate: synergistic effects and mechanisms, Environ. Sci. Technol. 50 (2016) 3119–3127.
[29] W.-D. Oh, Z. Dong, T.-T. Lim, Generation of sulfate radical through heterogeneous catalysts for organic contaminants removal: current development, challenges and prospects, Appl. Catal. B 194 (2016) 169–201.
[30] D. Tang, G. Zhang, S. Guo, Efficient activation of peroxymonosulfate by manganese oxide for the degradation of azo dye at ambient condition, J. Colloid Interface Sci. 454 (2015) 44–51.
[31] G.P. Anipsitakis, D.D. Dionysiou, Radical generation by the interaction of transition metals with common oxidants, Environ. Sci. Technol. 38 (2004) 3705–3712.
[32] J.A. Zazo, J.A. Casas, A.F. Mohedano, J.J. Rodríguez, Catalytic wet peroxide oxidation of phenol with a Fe/active carbon catalyst, Appl. Catal. B 65 (2006) 261–268.